

Superconducting and dynamically stable polymorphs of elemental calcium predicted under high pressure

Akinwumi Akinpelu and Yansun Yao

Citation: Chin. Phys. B, 2026, 35 (**5**): 057102. DOI: 10.1088/1674-1056/ae27b7
http://cpb.iphy.ac.cn; http://iopscience.iop.org/cpb

What follows is a list of articles you may be interested in

Anionic electron dimensionality and monolayer ferromagnetism in Y-Co electrides

Lu Zheng(郑璐), Zimeng Lv(吕梓萌), Xiaochen Huang(黄小琛), Zhuangfei Zhang(张壮飞), Chao Fang(房超), Yuewen Zhang(张跃文), Qianqian Wang(王倩倩), Liangchao Chen(陈良超), Xiaopeng Jia(贾晓鹏), Biao Wan(万彪), and Huiyang Gou(缑慧阳)

Chin. Phys. B, 2025, 34 (**9**): 097105. DOI: 10.1088/1674-1056/adf82f

Strain-modulated superconductivity of monolayer Tc_2B_2

Zhengtao Liu(刘正涛), Zihan Zhang(张子涵), Hao Song(宋昊), Tian Cui(崔田), and Defang Duan(段德芳)

Chin. Phys. B, 2025, 34 (**4**): 047104. DOI: 10.1088/1674-1056/adb94d

Insights to unusual antiferromagnetic behavior and exchange coupling interactions in $Mn_{23}C_6$

Ze-Kun Yu(于泽坤), Chao Zhou(周超), Kuo Bao(包括), Zhao-Qing Wang(王兆卿), En-Xuan Li(李恩萱), Jin-Ming Zhu(朱金铭), Yuan Qin(秦源), Yu-Han Meng(孟钰涵), Pin-Wen Zhu(朱品文), Qiang Tao(陶强), and Tian Cui(崔田)

Chin. Phys. B, 2025, 34 (**3**): 037101. DOI: 10.1088/1674-1056/adaadd

Unveiling the pressure-driven metal-semiconductor-metal transition in the doped TiS_2

Jiajun Chen(陈佳骏), Xindeng Lv(吕心邓), Simin Li(李思敏), Yaqian Dan(但雅倩), Yanping Huang(黄艳萍), and Tian Cui(崔田)

Chin. Phys. B, 2024, 33 (**6**): 067104. DOI: 10.1088/1674-1056/ad4325

The role of CALYPSO in the discovery of high-T_c hydrogen-rich superconductors

Wenwen Cui(崔文文), Yinwei Li(李印威)

Chin. Phys. B, 2019, 28 (**10**): 107104. DOI: 10.1088/1674-1056/ab4253

SPECIAL TOPIC — John Tse: Pioneer in high-pressure materials science

Superconducting and dynamically stable polymorphs of elemental calcium predicted under high pressure

Akinwumi Akinpelu and Yansun Yao[†]

Department of Physics and Engineering Physics, University of Saskatchewan, Saskatoon, Saskatchewan, S7N 5E2, Canada

(Received 31 October 2025; revised manuscript received 30 November 2025; accepted manuscript online 4 December 2025)

Compressed calcium undergoes successive structural transitions under high pressure. In this study, high-pressure polymorphs of elemental calcium were investigated using a machine-learned interatomic potential combined with a sensible random structure search. Two new energetically favourable and dynamically stable phases were predicted, crystallizing in the $P\text{-}42_1c$ and $P\text{-}31c$ space groups at high pressure. Both structures are predicted to be metallic and likely exhibit phonon-mediated superconductivity. Using the Allen-Dynes modified McMillan equation, the superconducting critical temperatures (T_c) were estimated to be 26 K for the $P\text{-}42_1c$ phase at 200 GPa and 31 K for the $P\text{-}31c$ phase at 250 GPa, which are comparable to the highest experimentally observed T_c for calcium (29 K at 216 GPa). These relatively high T_c values are attributed to strong electron–phonon coupling between partially occupied d states and moderate-frequency phonon modes. These findings provide further insight into the complex polymorphism and superconductivity of elemental calcium under extreme conditions.

Keywords: crystal structure prediction, phase changes, high pressure, material science, superconductivity

PACS: 71.20.Dg, 71.20.–b, 74.62.Fj, 61.50.Ks

DOI: 10.1088/1674-1056/ae27b7 **CSTR:** 32038.14.CPB.ae27b7

1. Introduction

The crystal structures of elemental metals tend to undergo a specific sequence of changes under increasing pressure. It was once expected that compressing metals would always favor a close-packed structure, where atoms occupy $\sim 74\%$ of the space. However, this assumption, based on rigid spherical atom models, does not always hold. High pressure can give access to otherwise unoccupied electronic states, leading to orbital hybridization and new bonding that destabilize close-packed structures.[1] Elemental calcium (Ca) provides a striking example of such behavior: instead of becoming more densely packed, Ca evolves from face-centered cubic (fcc) to body-centered cubic (bcc), and then to simple cubic (sc) under pressure, exhibiting a decreasing coordination number. First-principles calculations show that under pressure, solid calcium exhibits an increasing occupation of the d-band due to s–d electron transfer, in which electrons migrate from the s orbital to the initially empty d orbital.[2] This electronic transition, driven by pressure-induced reordering of orbital energies, significantly alters the electron-lattice interaction of Ca under high pressure.

Calcium is a reactive metal that appears dull and silvery when pure. As the third most abundant metal in the Earth's crust, it plays a crucial role in both geological and biological systems. Beyond these interests, calcium has also attracted intense attention for its rich sequence of structural transitions and superconducting behavior under pressure. Notably, more than 50 elements have been shown to exhibit superconductivity at ambient or high pressures,[3] but few exhibit the combination of structural diversity and high superconducting critical temperature (T_c) found in Ca.

At atmospheric pressure, calcium takes the form of a fcc structure (Ca I), which transforms into a bcc structure (Ca II) at 20 GPa.[4] Intriguingly, Ca-II was observed to transform into the sc structure (Ca III) at 32 GPa and room temperature.[4,5] Due to its low coordination and poor packing efficiency, the sc structure is extremely rare among elemental metals, with polonium being the only other known example. The stability of this sc phase in Ca remained a puzzle for a while, as quasiharmonic phonon calculations indicated that its lattice dynamics have imaginary phonon frequencies, which suggests dynamic instability.[6–8] Subsequent theoretical study[9] reconciles this discrepancy by predicting a low-temperature structure isostructural to β-Sn, crystallizing in the $I4_1/amd$ space group, which becomes energetically favorable over sc near 34 GPa. This prediction was later confirmed experimentally at temperatures below 7 K.[10] Further compression induces structural transitions to Ca-IV and Ca-V, which were found to be a tetragonal $P4_12_12$ structure with fourfold helical atomic arrangements and an orthorhombic $Cmca$ structure with zigzag atomic arrangements, respectively.[11] These phases were observed experimentally, and the measured structures closely matched prior theoretical predictions.[12,13] Fur-

[†]Corresponding author. E-mail: yansun.yao@usask.ca

© 2026 Chinese Physical Society and IOP Publishing Ltd. All rights, including for text and data mining, AI training, and similar technologies, are reserved.

thermore, calcium undergoes a structural phase transition to the *Pnma* (Ca VI) structure at pressures ranging between 117–135 GPa,[14] then transforms into a chain-ordered host-guest structure, $I4/mcm$ (Ca VII) above 135 GPa.[15] The observed Ca VI and Ca VII are consistent with prior theoretical predictions.[12,16–18] Ca-VII was observed experimentally around 210 GPa and exhibits a T_c of 29 K at 216 GPa,[19] which, as of 2011, was the highest confirmed T_c among all elemental superconductors. This record was later surpassed in 2023, when a T_c of 33 K was measured in scandium at 260 GPa.[20] These pressure-induced transformations to crystallographically lower symmetry structures are strongly influenced by s–d electron transfer, which dictates the electronic structure and bonding patterns of Ca under pressure. Calcium's unusual richness of high-pressure phases and its superconducting behavior have always sparked intense experimental and theoretical research.

In the present work, we present two novel high-pressure phases of calcium that are identified using advanced structure search techniques. A comprehensive search was conducted at multiple pressures across a polymorphic space of over 500000 randomly generated candidate structures, sampling all possible space groups. The calculation was accelerated using a data-derived interatomic potential[21,22] within a sensible random structure search approach.[23,24] Similar methodologies have been successfully applied in a variety of materials problems, including the microscopic theory of color in lutetium hydride,[25] the search for ambient superconductivity in the Lu–H–N system,[26] the prediction of a metastable ambient-pressure hydride superconductor, Mg_2IrH_6, with a predicted T_c of 160 K,[27] uncovering a previously unseen thermodynamically stable structure of SiH_4 with 12 formula units,[21] the prediction of direct bandgap allotropes of germanium,[28] and the resolution of the crystal structure of the tI50 phase of sodium.[29] Our approach combines (sensible) random structure generation, screening, and optimization using data-driven interatomic potentials, and fine evaluation with density functional theory (DFT)[30,31] calculations. With this search, we report two new energetically competitive phases of Ca at high pressure: a primitive tetragonal structure (P-42_1c) with 10 atoms per unit cell, and a primitive trigonal (aP20) structure (P-$31c$) with 20 atoms per unit cell. Both phases are predicted to be phonon-mediated superconductors. In particular, the P-$31c$ phase has a stronger electron–phonon coupling strength driven by enhanced interactions between d electrons and moderate-frequency phonons, which is responsible for its high predicted T_c.

2. Methods and computational details

2.1. Structure search

Structural searches were performed using the *ab initio* random structure search (AIRSS) method[23,24] and code,[32] combined with a machine-learned interatomic potential (MLIP), which utilizes a set of shallow neural networks[21,22] for structural optimization. Construction of the MLIP is done using the ephemeral data-derived potentials (EDDP) package[33] through iterative exploration of the configuration space without any prior knowledge of known structures. The potential training was performed in six iterative cycles. The initial potential model was trained using a dataset of 2000 randomly generated structures. In each subsequent iteration, around 1150 newly generated structures optimized using the current potential were added to the training set. After rejecting unphysical structures, this iterative process produced a final dataset of 7911 structures on which the final potential was trained. Out of 520 individual neural network fits, 13 were selected by non-negative least squares (NNLS) to construct the potential. For the EDDP training, unit cells with 8 Ca atoms were employed, while the AIRSS search for Ca structures used various unit cell sizes containing up to 20 atoms. The parameters for random structure generation included a volume range of 10.0–26.0 Å^3/atom, a cut-off radius of 6.0 Å, function exponents ranging from 2 to 10, and features accounting for up to three-body interactions. The minimum interatomic separation was constrained between 1.5 Å and 3.5 Å to avoid unphysical geometries. Both the potential generation and structure search were conducted at two pressures, 200 GPa and 250 GPa. Candidate structures were generated with up to 48 symmetry operations corresponding to a search across randomly selected space groups. From the search results, several distinct low-enthalpy structures were selected for further analysis.

2.2. Computational details

A multi-step optimization strategy was used to relax the 248 most stable structures predicted at 200 GPa and the 174 most stable structures at 250 GPa using the Vienna *ab initio* simulation package (VASP).[34] The Perdew–Burke–Ernzerhof (PBE) exchange–correlation functional[35] was used in conjunction with a plane wave basis set with an energy cutoff of 266 eV. Brillouin zone sampling was performed using Monkhorst–Pack k-point meshes[36] with a spacing of $2\pi \times 0.032$ Å^{-1} that proved to give excellent convergence of the stress tensor and energy. The self-consistent calculations were considered converged when the energy change fell below 10^{-8} eV/atom, and all structures were optimized until the Hellmann–Feynman forces on atoms were reduced to below 1 meV/Å. Enthalpy, electronic band structure, and density of states calculations were performed using VASP with a 10-electron ($3s^23p^64s^2$) PAW potential[37] with the PBE

functional. Phonon dispersion relations were calculated using density functional perturbation theory (DFPT)[38] as implemented in VASP and post-processed using the Phonopy package.[39] The electron localization function and topological critical points were analyzed using the quantum theory of atoms in molecules (AIM)[40] as implemented in the CRITIC2 program.[41] Electron–phonon coupling (EPC) calculations were performed using the Quantum ESPRESSO package,[42] with a 10-electron ultrasoft pseudopotential[43] with nonlinear core corrections. The EPC matrices were evaluated in the first Brillouin zone on a $4\times4\times4$ q-grid with individual EPC matrices obtained with a $16\times16\times16$ k-grid and a Gaussian smearing width of 0.05 Ry. The superconducting critical temperature T_c was estimated using the Allen-Dynes-modified McMillan equation[44,45] with a renormalized Coulomb pseudopotential $\mu^*=0.10$. Crystal structures were visualized using the visualization for electronic structural analysis (VESTA) tool.[46]

3. Results and discussion

Structural searches successfully recovered all previously observed structures of elemental calcium (fcc, bcc, sc, $I4_1/amd$, $P4_12_12$, $Cmca$, $Pnma$, and $I4/mcm$) and revealed two new energetically competitive phases: a primitive tetragonal structure with 10 atoms per unit cell in the P-42_1c space group, and a primitive trigonal structure with 20 atoms per unit cell in the P-$31c$ space group. The optimized structural parameters of the P-42_1c and P-$31c$ phases are listed in Table 1, and their crystal structures are illustrated in Figs. 1(a) and 1(b), respectively. The enthalpies of the most energetically competitive structures are compared over the pressure range up to 250 GPa, as displayed in Fig. 1(c). At 200 GPa, the structural parameters for the P-42_1c structure converge to $a=4.6425$ Å, $c=4.3003$ Å, with Ca atoms located at 8e and 2b Wyckoff sites. Likewise, at 250 GPa, the P-$31c$ structure converges to $a=7.3954$ Å, $c=3.6782$ Å, and $\gamma=120°$, with Ca atoms at 12i, 6h, and 2d sites. To investigate their thermodynamic stability, the enthalpies of the two new phases were calculated and compared to those of known ground-state structures up to 250 GPa, with fcc used as the reference. As shown in Fig. 1(c), the P-42_1c phase is among the most stable structures in the 100–150 GPa range, reaching its minimum enthalpy (relative to fcc) around 125 GPa. At 110 GPa, its most stable point, its enthalpy is only 14 meV/atom above the ground state, suggesting it could be thermodynamically stabilized under suitable conditions. The P-31c phase, while not the thermodynamic ground state at any pressure, exhibits enthalpies nearly identical to those of the sc structure up to $\sim$60 GPa, and becomes energetically more favorable at higher pressures. Notably, the sc phase is also not the ground state, but it has been observed experimentally at room temperature between 32 GPa and 109 GPa.[4,5] The fact that the P-31c phase matches or even slightly surpasses the sc phase in enthalpy strongly suggests that it too could be experimentally accessible. These findings point to both P-42_1c and P-31c as viable metastable structures with a realistic chance of realization under high-pressure conditions.

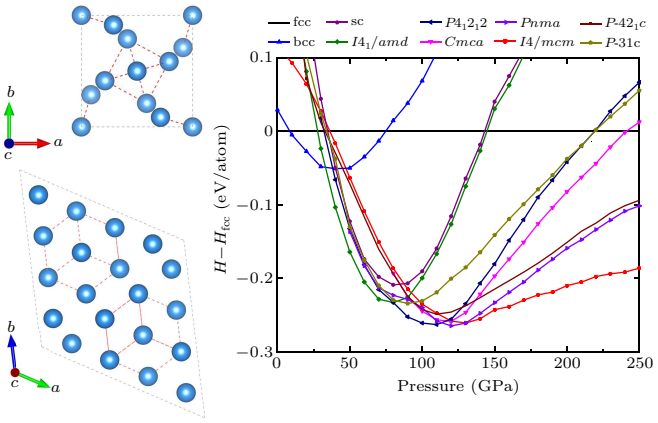


Fig. 1. Optimized crystal structures of the predicted Ca phases, (a) P-42_1c structure and (b) P-31c structure viewed along the c-axis. The calcium atoms are colored blue. The red dashed lines represent the interatomic bond lengths. (c) Enthalpies of predicted and previously known Ca structures up to 250 GPa. The enthalpy of the fcc phase is used as the reference.

Table 1. Optimized structural parameters for the predicted structures of the P-42_1c and P-31c phases.

Space group (SG)	Pressure (GPa)	Lattice parameters (Å)	Atomic fractional coordinates			
P-42_1c	200	$a=4.6425$, $c=4.3003$	8e	0.4138	0.7886	0.3881
			2b	0.0000	0.0000	0.5000
P-31c	250	$a=7.3954$, $c=3.6782$, $\gamma=120°$	12i	0.5669	0.8991	0.4161
			6h	0.8988	0.1012	0.2500
			2d	0.6667	0.3333	0.2500

The electron localization function (ELF)[47] was employed to examine the electronic structures of the predicted calcium phases. The ELF takes values between 0 and 1, where 1.0 corresponds to perfect localization, while 0.5 corresponds to the localization level of a uniform electron gas, representing moderate electron localization. Figures 2(a) and 2(b) show the ELF distributions for the P-42_1c and P-31c structures at 200 GPa and 250 GPa, respectively. In the P-42_1c structure, the ELF decreases monotonically from 1 near the calcium nuclei to nearly 0 in the interstitial regions, indicating closed-shell behavior with no signs of interatomic electron localization, which is consistent with metallic bonding.

In the *P*-31*c* structure, while a slight increase in ELF is observed between calcium atoms, the values remain too low to suggest the presence of covalent bonds or electride-like electron accumulations.[48,49] This subtle feature instead suggests a weak tendency for electron accumulation in interstitial regions, again consistent with moderately delocalized metallic bonding.

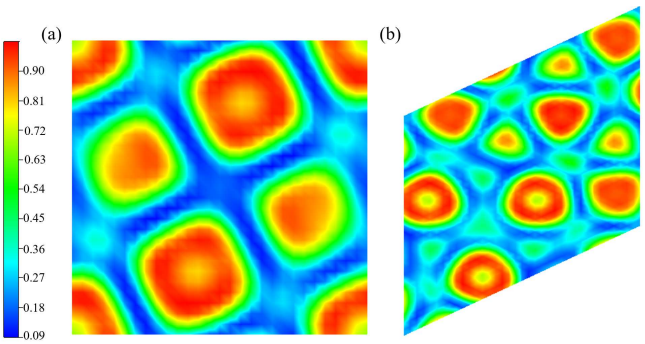


Fig. 2. ELF contour map showing the (a) (0 0 1) plane of the *P*-42$_1$*c* phase at 200 GPa and (b) (0 0 1) plane of the *P*-31*c* phase at 250 GPa.

To further understand the bonding in the predicted phases, we performed a topological analysis of the electron density using the quantum theory of atoms in molecules (QTAIM).[50,51] This analysis complements the ELF results by providing a qualitative description of interatomic interactions via the identification of critical points (CPs), where the gradient of the electron density vanishes. There are primarily four types of CPs classified by two indices: one denotes the number of non-zero principal curvatures, where -1 denotes a local maximum and $+1$ a local minimum, and the other is their sum. Specifically, nuclear CPs (3, -3) are maxima at atomic nuclei; bond CPs (3, -1) occur along bond paths between atoms, where the electron density is a maximum in the bonding plane but a minimum perpendicular to it; ring CPs (3, $+1$) are found in ring structures; and cage CPs (3, $+3$) appear in enclosed voids as local minima.

At 200 GPa, the *P*-42$_1$*c* structure exhibits four distinct CPs between calcium atoms (Fig. S1 of the supporting information). The electron density ρ at these CPs has values ranging from 0.4264 $e^-\cdot$Å^{-3} to 0.6120 $e^-\cdot$Å^{-3}, with corresponding Laplacian $\nabla^2\rho$ between 7.7485 $e^-\cdot$Å^{-5} and 11.4977 $e^-\cdot$Å^{-5}. The positive $\nabla^2\rho$ is characteristic of closed-shell interactions in metallic systems, and the values are typical for metallic bonding, i.e., slightly stronger than hydrogen bonding.[52] Additional properties at these CPs, including the kinetic (G), potential (V), and total ($E = G + V$) energy densities, are listed in Table S1. Since G is always positive and V is always negative, their small negative sum (E) indicates weak but stabilizing interactions due to partial electron sharing from overlapping states with a preference along the Ca–Ca paths. A similar bonding picture is revealed in the *P*-31*c* structure at 250 GPa, where ρ at the CPs slightly increases to 0.4975–0.6822 $e^-\cdot$Å^{-3}, and $\nabla^2\rho$ remains positive in the range 8.0012–11.4412 $e^-\cdot$Å^{-5}. These values again point to weak, delocalized metallic bonding. Full topological parameters for this structure are provided in Table S2.

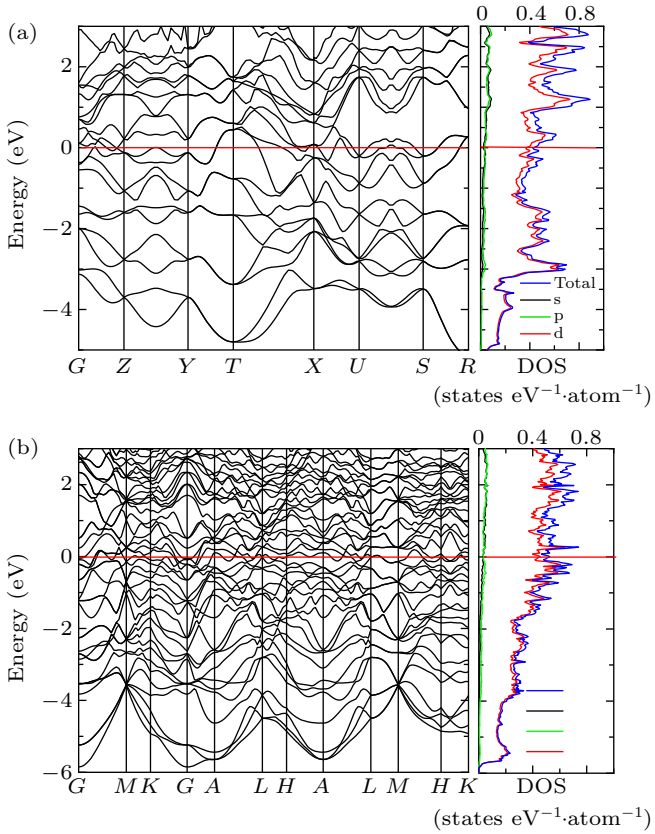


Fig. 3. Band structure and projected density of states of (a) the *P*-42$_1$*c* structure at 200 GPa and (b) the *P*-31*c* phase at 250 GPa. The Fermi level is shifted to 0 eV, as indicated by the red line.

Figure 3 (left) shows the calculated band structure and projected densities of states (DOS) for s, p, and d orbitals of the *P*-42$_1$*c* structure at 200 GPa. The band structure shows several bands crossing the Fermi level, confirming its metallic behavior. Interestingly, there are occasions where almost parallel bands cross the Fermi level, for instance along the $\Gamma \to Z$, $T \to X$, $X \to U$, and $S \to R$ paths. Parallel bands crossing the Fermi level are signs of possible nesting of two portions of the Fermi surface (FS), a feature known to create "hot zones" in the Brillouin zone that are favorable for the formation of Cooper pairs.[53,54] Additionally, some bands near the Fermi level appear relatively flat in certain regions, which further enhances this effect by increasing the DOS where phonons can couple most effectively.[55,56] The DOS at the Fermi level is dominated by d-orbital contributions, with minimal s and p contributions, revealing a pronounced pressure-induced s to d electronic transition. Under high pressure, the s-band shifts upward in energy due to increased Coulomb repulsion, while the d-band shifts downward, facilitating electron transfer from s to d orbitals.[16] This behavior is common in alkali and alkaline earth metals and governs many of calcium's structural transitions, including the bcc to sc phase change.[2] Below

−3 eV, the DOS is almost entirely attributed to d-orbitals, indicating strong d-electron participation in the valence region. Figure 3 (right) shows the electronic structure of the P-31c phase at 250 GPa. Like the P-42$_1c$ structure, it exhibits metallic character with a complex band structure and a high DOS of d-electron states near the Fermi level, again indicating a strong s to d transition under extreme pressure. The overall DOS at the Fermi level is slightly higher than that of the P-42$_1c$ structure. The presence of multiple flat bands in its band structure suggests reduced electron mobility compared to more dispersive phases, which may enhance electronic correlations and instabilities such as superconductivity.[57]

Subsequently, to explore the possibility of phonon-mediated superconductivity, the phonon linewidths and the EPC parameter λ, defined as the first reciprocal moment of the Eliashberg phonon spectral function $\alpha^2F(\omega)$, were calculated using the perturbative linear response method within density functional perturbation theory. The superconducting critical temperature T_c was then estimated via the Allen–Dynes modified McMillan equation[44,45]

$$T_c = \frac{\omega_{\log}}{1.2}\exp\left[-\frac{1.04(1+\lambda)}{\lambda-\mu^*(1+0.62\lambda)}\right]. \quad (1)$$

The phonon dispersion, phonon density of states (PhDOS), and Eliashberg spectral function $\alpha^2F(\omega)$ of the P-42$_1c$ phase at 200 GPa are shown in Fig. 4. The absence of imaginary phonon frequencies across the Brillouin zone indicates that the structure is dynamically stable and potentially synthesizable under high-pressure conditions. Unlike multielement compounds, where phonon modes often separate into distinct blocks due to differences in atomic masses, the phonon branches in elemental calcium are uniformly distributed across the spectrum without clear frequency groupings. This continuous phonon distribution reflects the homogeneous nature of the lattice dynamics. As such, $\alpha^2F(\omega)$ shows a relatively even distribution over the frequencies where the phonon DOS is appreciable. However, due to the inverse-frequency (ω^{-1}) weighting in the electron–phonon coupling integral, the low- to mid-frequency modes contribute more significantly to the EPC strength λ. This yields a strong electron–phonon coupling constant of $\lambda = 1.03$, which is considered very high for an elemental system. Using a Coulomb pseudopotential $\mu^* = 0.1$ in the Allen–Dynes formula, the superconducting critical temperature is estimated to be $T_c = 26.04$ K.

The superconducting T_c of calcium has been predicted to increase with increasing occupancy of d electrons[16] and may continue to increase across successive high-pressure structural phases.[58] For the P-31c phase at 250 GPa, the phonon dispersion, PhDOS, and $\alpha^2F(\omega)$ confirm both dynamical stability and strong electron–phonon coupling (Fig. 5). The PhDOS and $\alpha^2F(\omega)$ show that the strong electron–phonon coupling mainly originates from moderate-frequency phonons, which contribute more than 90% of the total EPC strength. The resulting EPC constant is $\lambda = 1.39$. With a Coulomb pseudopotential value of $\mu^* = 0.1$, the estimated T_c is 31.0 K. This elevated T_c is attributable to strong coupling between electrons in the partially occupied Ca d orbitals and mid-frequency phonons. To date, the highest experimentally observed T_c for elemental calcium under pressure is 29 K at 216 GPa.[11] Our predicted value of 31 K at 250 GPa for the P-31c phase is comparable and suggests that calcium may host additional superconducting phases in different crystal structures.

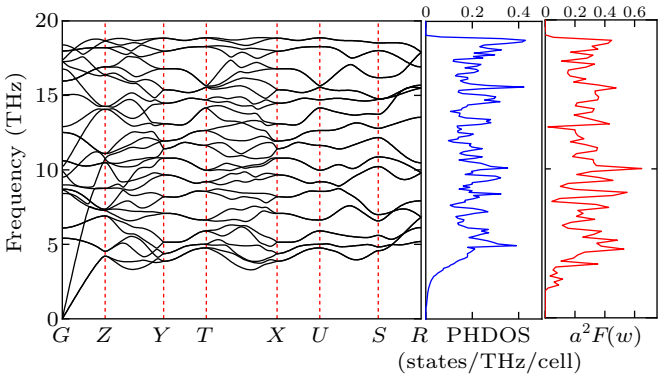


Fig. 4. Phonon dispersion curves, PhDOS, and Eliashberg phonon spectral function $\alpha^2F(\omega)$ of calcium in the P-42$_1c$ phase at 200 GPa.

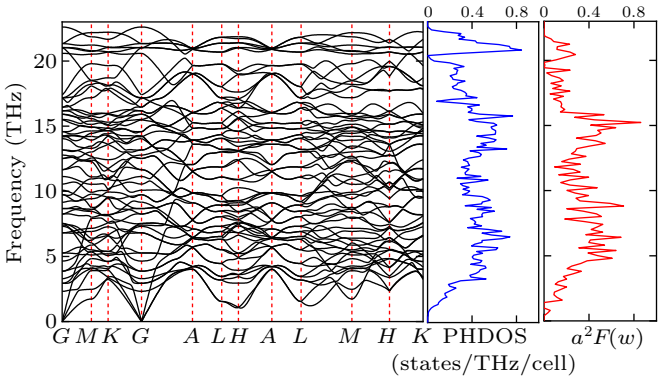


Fig. 5. Phonon dispersion curves, PhDOS, and Eliashberg phonon spectral function $\alpha^2F(\omega)$ of calcium in the P-31c phase at 250 GPa.

4. Summary

In summary, a machine-learned interatomic potential was employed to accelerate the crystal structure search, which led to the prediction of two energetically favorable high-pressure phases of elemental calcium. These include a primitive tetragonal phase P-42$_1c$ with 10 atoms per unit cell and a primitive trigonal phase P-31c with 20 atoms per unit cell. Electronic structure calculations establish the metallic nature of both phases, which was further supported by topological analysis of the electron density. Phonon and electron–phonon coupling calculations indicate that both structures are dynamically stable and potentially exhibit phonon-mediated superconductivity. The superconducting critical temperatures (T_c) were estimated to be 26 K for the P-42$_1c$ phase at 200 GPa and 31 K

for the *P*-31*c* phase at 250 GPa. These values are comparable to the highest experimentally reported T_c for elemental calcium (29 K at 216 GPa) and among the highest predicted T_c values for elemental materials under high pressure.

Acknowledgments

Project supported by the Information and Communications Technology group and the High-Performance Computing Training and Research Facilities at the University of Saskatchewan for the use of the Plato cluster computing resource, as well as computing clusters provided by West Grid and Digital Research Alliance of Canada. This project was supported by the Natural Sciences and Engineering Research Council of Canada (NSERC).

References

[1] Grochala W, Hoffmann R, Feng J and Ashcroft N W 2007 *Angew. Chem. Int. Ed.* **46** 3620
[2] Ahuja R, Eriksson O, Wills J M and Johansson B 1995 *Phys. Rev. Lett.* **75** 3473
[3] Hamlin J J 2015 *Physica C* **514** 59
[4] Olijnyk H and Holzapfel W B 1984 *Phys. Lett. A* **100** 191
[5] Yabuuchi T, Nakamoto Y, Shimizu K and Kikegawa T 2005 *J. Phys. Soc. Jpn.* **74** 2391
[6] Teweldeberhan A M and Bonev S A 2008 *Phys. Rev. B* **78** 140101
[7] Gao G, Xie Y, Cui T, Ma Y, Zhang L and Zou G 2008 *Solid State Commun.* **146** 181
[8] Yao Y, Martoňák R, Patchkovskii S and Klug D D 2010 *Phys. Rev. B* **82** 094107
[9] Yao Y, Klug D D, Sun J and Martoňák R 2009 *Phys. Rev. Lett.* **103** 055503
[10] Li B, Ding Y, Yang W, Wang L, Zou B, Shu J, Sinogeikin S, Park C, Zou G and Mao H K 2012 *Proc. Natl. Acad. Sci. USA* **109** 16459
[11] Fujihisa H, Nakamoto Y, Shimizu K, Yabuuchi T and Gotoh Y 2008 *Phys. Rev. Lett.* **101** 095503
[12] Yao Y, Tse J S, Song Z, Klug D D, Sun J and Le Page Y 2008 *Phys. Rev. B* **78** 054506
[13] Ishikawa T, Ichikawa A, Nagara H, Geshi M, Kusakabe K and Suzuki N 2008 *Phys. Rev. B* **77** 020101
[14] Nakamoto Y, Sakata M, Shimizu K, Fujihisa H, Matsuoka T, Ohishi Y and Kikegawa T 2010 *Phys. Rev. B* **81** 140106
[15] Fujihisa H, Nakamoto Y, Sakata M, Shimizu K, Matsuoka T, Ohishi Y, Yamawaki H, Takeya S and Gotoh Y 2013 *Phys. Rev. Lett.* **110** 235501
[16] Oganov A R, Ma Y, Xu Y, Errea I, Bergara A and Lyakhov A O 2010 *Proc. Natl. Acad. Sci. USA* **107** 7646
[17] Arapan S, Mao H K and Ahuja R 2008 *Proc. Natl. Acad. Sci. USA* **105** 20627
[18] Ishikawa T, Nagara H, Suzuki N, Tsuchiya T and Tsuchiya J 2010 *Phys. Rev. B* **81** 092104
[19] Sakata M, Nakamoto Y, Shimizu K, Matsuoka T and Ohishi Y 2011 *Phys. Rev. B* **83** 220512
[20] Ying J, Liu S, Lu Q, Wen X, Gui Z, Zhang Y, Wang X, Sun J and Chen X 2023 *Phys. Rev. Lett.* **130** 256002
[21] Pickard C J 2022 *Phys. Rev. B* **106** 014102
[22] Salzbrenner P T, Joo S H, Conway L J, Cooke P I C, Zhu B, Matraszek M P, Witt W C and Pickard C J 2023 *J. Chem. Phys.* **159** 144801
[23] Pickard C J and Needs R J 2006 *Phys. Rev. Lett.* **97** 045504
[24] Pickard C J and Needs R J 2011 *J. Phys.: Condens. Matter* **23** 053201
[25] Kim S W, Conway L J, Pickard C J, Pascut G L and Monserrat B 2023 *Nat. Commun.* **14** 7360
[26] Ferreira P P, Conway L J, Cucciari A, Di Cataldo S, Giannessi F, Kogler E, Eleno L T F, Pickard C J, Heil C and Boeri L 2023 *Nat. Commun.* **14** 5367
[27] Dolui K, Conway L J, Heil C, Strobel T A, Prasankumar R P and Pickard C J 2024 *Phys. Rev. Lett.* **132** 166001
[28] Bhullar M, Akinpelu A and Yao Y 2024 *Comput. Mater. Today* **3** 100009
[29] Akinpelu A, Bhullar M, Wang H and Yao Y 2025 *Commun. Chem.* **8** 177
[30] Hohenberg P and Kohn W 1964 *Phys. Rev.* **136** B864
[31] Kohn W and Sham L J 1965 *Phys. Rev.* **140** A1133
[32] https://www.mtg.msm.cam.ac.uk/Codes/AIRSS
[33] https://www.mtg.msm.cam.ac.uk/Codes/EDDP
[34] Kresse G and Furthmüller J 1996 *Phys. Rev. B* **54** 11169
[35] Perdew J P, Burke K and Ernzerhof M 1996 *Phys. Rev. Lett.* **77** 3865
[36] Monkhorst H J and Pack J D 1976 *Phys. Rev. B* **13** 5188
[37] Blöchl P E 1994 *Phys. Rev. B* **50** 17953
[38] Baroni S, de Gironcoli S, Dal Corso A and Giannozzi P 2001 *Rev. Mod. Phys.* **73** 515
[39] Togo A, Oba F and Tanaka I 2008 *Phys. Rev. B* **78** 134106
[40] Bader R F W 1991 *Chem. Rev.* **91** 893
[41] Otero-de-la-Roza A, Johnson E R and Luãna V 2014 *Comput. Phys. Commun.* **185** 1007
[42] Giannozzi P, Baroni S, Bonini N, Calandra M, Car R, Cavazzoni C, Ceresoli D, Chiarotti G L, Cococcioni M, Dabo I 2009 *J. Phys.: Condens. Matter* **21** 395502
[43] Vanderbilt D 1990 *Phys. Rev. B* **41** 7892
[44] McMillan W L 1968 *Phys. Rev.* **167** 331
[45] Allen P B and Dynes R C 1975 *Phys. Rev. B* **12** 905
[46] Momma K and Izumi F 2011 *J. Appl. Crystallogr.* **44** 1272
[47] Becke A D and Edgecombe K E 1990 *J. Chem. Phys.* **92** 5397
[48] Racioppi S and Zurek E 2025 *Acta Cryst. B* **81** 256
[49] Racioppi S, Storm C V, McMahon M I and Zurek E 2023 *Angew. Chem. Int. Ed.* **62** e202310802
[50] Bader R F W and Esseén H 1984 *J. Chem. Phys.* **80** 1943
[51] Bader R F W, MacDougall P J and Lau C D 1984 *J. Am. Chem. Soc.* **106** 1594
[52] Yao Y, Yong X, Tse J S and Greschner M J 2014 *J. Phys. Chem. C* **118** 29591
[53] Kasinathan D, Kuneš J, Lazicki A, Rosner H, Yoo C S, Scalettar R T and Pickett W E 2006 *Phys. Rev. Lett.* **96** 047004
[54] Tse J S, Yao Y and Tanaka K 2007 *Phys. Rev. Lett.* **98** 117004
[55] Simon A 1997 *Angew. Chem. Int. Ed.* **36** 1788
[56] Majumdar A, Tse J S and Yao Y 2017 *Angew. Chem. Int. Ed.* **56** 11390
[57] Yao Y, Tse J S, Tanaka K, Marsiglio F and Ma Y 2009 *Phys. Rev. B* **79** 054524
[58] Matsuoka T, Nakamoto Y and Shimizu K 2006 *J. Phys. Soc. Jpn.* **75** 083703